Polymer Journal, Vol. 12, No. 4, pp 251—264 (1980)

Rheo-Optical Studies on the Deformation Mechanism of Semicrystalline Polymers. XI. Mechanical and Optical Retardation Spectra of a High-Density Polyethylene Having Row-Nucleated Crystalline Texture of *c*-Axis Orientation

Thein KYU, Shoji SUEHIRO, and Hiromichi KAWAI*

Department of Polymer Chemistry, Faculty of Engineering, Kyoto University, Yoshida, Sakyo-ku, Kyoto 606, Japan.

(Received November 17, 1979)

ABSTRACT: The frequency dispersions of the dynamic birefringence and dynamic mechanical compliance functions of a high-density polyethylene film having a row-nucleated crystalline texture of preferential *c*-axis orientation along the machine direction were investigated over a frequency range from 0.008 to 4.3 Hz at various temperatures from 20 to 110°C. Two dispersions corresponding to the α_1 and α_2 processes were observed in the mechanical data. The resolution of these two processes in the frequency dispersion of the loss compliance function was carried out for the MD (machine direction) specimen and TD (transverse direction) specimen, quantitatively. From these resolved loss compliance master curves, the corresponding mechanical retardation time spectra were computed by a deconvolution method. It was found that the α_1 retardation time spectra for both specimens appear at approximately the same retardation time range with almost equal peak intensity as well as integrated intensity, whereas the α_2 retardation time spectrum of the TD specimen appeared at a longer time range with larger integrated intensity than that of the MD specimen. Subsequently, it is concluded that the α_2 process is more conspicuous in the TD specimen than in the MD specimen. In the dynamic birefringence results, only one dispersion, whose activation energy is comparable with that of the α_1 mechanical dispersion, was observed in both specimens. The optical retardation time spectra computed also by the deconvolution method from the master curve of the imaginary component of stress-optical coefficient function, were found to be more prominent and to appear at a longer retardation time range for the TD specimen than for the MD specimen. These spectral peak positions on the retardation time scale do not correspond to those of the α_1 mechanical spectra in both specimens.

KEY WORDS Rheo-Optics / Row-Nucleated Polyethylene / Deformation Mechanism / Mechanical and Optical Retardation Spectra /

In an effort to understand the structural origin of the α mechanical dispersion of polyethylene, a calendered high-density polyethylene film having a row-nucleated crystalline texture of preferential *c*-axis orientation[1] has been used in previous studies of dynamic X-ray diffraction[2] and dynamic birefringence.[3] The choice of this calendered film has an advantage over the melt-crystallized ones having spherulitic crystalline texture, because of its much simpler crystalline morphology and, subsequently, is much more distinguishable in the deformation mechanisms of the textures against mechanical excitations. For example, the calendered film has a crystalline texture of cylindrical symmetry; *i.e.*, cylindrite rather than spherulite, along the machine direction of fabricating the film specimen, so that the dynamic studies of the structural responses against the mechanical excitations along the machine direction (MD) and transverse direction (TD) of the calendered film are expected to reveal the responses at the equatorial and polar zones of the spherulitic texture, respectively, against uniaxial excitations of the melt-crystallized spherulitic film specimen.

It was observed in a previous dynamic X-ray diffraction study that the α_1 dispersion corresponding to a lower temperature dispersion of the α mechanical dispersion was attributed to the lamellar

* To whom correspondence should be addressed.

detwisting process associated with rotation of crystal grains within the lamellae around the crystal *b*-axis in the MD specimen and the intralamellar shearing process associated with rotation of the grains around the crystal *a*-axis in the TD Specimen. These two fundamental deformation processes are believed to be associated with the α_1 dispersion of the melt-crystallized polyethylene possessing the spherulitic crystalline texture. Also, an additional deformation process of interlamellar splaying or lamellar bending concomitant to the negative form birefringence was found in the vicinity of α_1 dispersion of the MD specimen in the dynamic birefringence study.[3] However, its contribution to the α_1 process is not likely to be substantial, as it is in the β process and is believed to be more crucial to the high recoverability from large extensions or to the so-called hard elasticity when deformed along the MD. The prominant frequency dispersion in the complex dynamic crystal lattice compliance at relatively high temperatures supports the idea that the intracrystalline relaxation takes place in the vicinity of α_2 mechanical dispersion in the TD.[2]

All these fundamental responses were analyzed in terms of the strain-optical or strain-orientation coefficient functions in which the optical quantities of structural responses refer to the external bulk strain. As was pointed out in a previous paper,[4] the strain-optical coefficient functions may be of crucial importance to account for the deformation mechanism of the internal structures, but may not be rigorous for comparison with its counterpart functions; *i.e.*, the dynamic modulus function. Hence, the correspondence between the orientation dispersion processes observed from the strain-orientation function and the mechanical dispersion processes from the dynamic modulus function is still uncertain. Furthermore, the frequency dispersion of the complex dynamic modulus function of the row-nucleated polyethylene specimens was found to be composed of two components in the vicinity of the α mechanical dispersion; *i.e.*, the α_1 and α_2 mechanical dispersions with activation energies of around 25 and 35 kcal mol^{-1}, respectively. As far as the comparison between the optical and mechanical dispersions are concerned, the resolution of the mechanical dispersion into individual contributions in a quantitative manner must be essential. However, the quantitative separation of the frequency dispersion processes from apparent master curves of the loss modulus function was hindered by the fact that the dispersion peaks appear so close in the frequency regions as well as in their magnitudes, leading to a very broad and asymmetric frequency dispersion curve in the apparent master curves of loss modulus function.

In this paper, the above fundamental deformation processes are analyzed in terms of the stress-optical coefficient functions with emphasis on its correspondence to the elastic compliance function, rather than to the modulus function. First, the quantitative separation of the α mechanical dispersion into individual processes; *i.e.*, the α_1 and α_2 processes, are performed for the frequency dispersion of loss compliance functions at various temperatures, based on the resolution procedure proposed by Kawai *et al.*[5,6] The mechanical retardation spectra of the resolved and unresolved (apparent) dispersions are evaluated from the loss compliance functions in accordance with the deconvolution method reported earlier by the present authors,[4] and are compared with the MD and TD specimens. Second, the optical retardation spectra are also computed by the deconvolution method from the superposed master curves of the stress-optical coefficient functions, and are compared with these two specimens as well as with the mechanical retardation spectra of the same specimens.

TEST SPECIMEN

An extra-high-molecular-weight linear polyethylene (Sholex Super 5551H, Japan Oleifin Chemical Ind., Ltd.) having a weight-averaged molecular weight of 350,000 was fed into a bumbery mixer where in the pellets were melted for several minutes. The melt, kept at *ca.* 160°C at the exit of the mixer, was also fed into the mixing rolls controlled at 150°C and then calendered into sheet form by passing it through a set of calender rolls. The temperature and relative surface velocity of these rolls were controlled so as to crystallize the melts under sufficiently high shear stress. The calendered films thus prepared had a density of 0.951 $g\,cm^{-3}$ and a volume-average degree of crystallinity of 66.6%, assuming the densities of the crystalline and amorphous phases to be 1.000 and 0.852 $g\,cm^{-3}$, respectively. The details of the fabrication processes and morphological characterizations of these film specimens are described elsewhere.[1]

EXPERIMENTAL PROCEDURE

Prior to the static and dynamic experiments, the above-mentioned film specimens were annealed by placing them between two polished stainless steel plates at 110°C for more than 5 hours in a vacuum oven in order to prevent undesirable thermal effects during the course of the experiments. For the dynamic birefringence measurement, the MD and TD specimens were cut from a calendered film of 200 μm thinkness into a ribbon shape 80 mm in length and 8 mm in width along the machine and transverse directions of frabrication, respectively. The ribbon-shape specimen was mounted on a tensile dynamic deformation apparatus at an initial gauge length of 60 mm and was subjected to a static tensile strain of 3.3% to avoid buckling of the specimen while imposing a dynamic tensile strain of 0.25%. A preparatory vibration was applied for about one hour at 4.3 Hz at the temperature of each measurements to assure a vibrational steady state and also to perform a sort of mechanical conditioning of the specimen. The simultaneous measurement of dynamic mechanical and dynamic birefringence behavior was conducted by means of a π-sector technique,[7] developed by one of the authors of this paper, over a frequency range from 0.008 to 4.3 Hz, at various temperature from 30 to 110°C.

RESULTS AND DISCUSSION

Morphological and Deformation Behavior under Static Elongation

According to the previous electron microscopic (EM) and small-angle X-ray scattering (SAXS) studies,[1] the above-mentioned calendered specimen possessed a crystalline texture of cylidrites in which stacks of crystal lamellae accompanied to some degree by lamellar twisting were oriented radially with their lamellar axes perpendicular to the machine direction of fabrication. These lamellae are considered to grow out from rows of nucleating points, as proposed by Keller and Machin,[8] to form a sort of lamellar network. The two-point SAXS pattern in the meridional direction (machine direction) of the unstretched specimen indicates the high degree of lamellar orientation in the transverse direction of the fabrication.

The cyclic tensile stress–strain behavior exhibits a high degree of length recoverability from a large extension along the machine direction, but such highly elastic behavior can not be observed when stretched in the transverse direction. Instead, the behavior is characterized by a discrete yielding phenomenon at a relatively small elongation, *ca.* 5% elongation, followed by a plastic deformation related to a macroscopic necking of the specimen. This high recoverability in the MD is believed to be an inherent property of the lamellar network morphology associated with the interlamellar spalying or lamellar bending process, like a leaf-spring, as suggested by several authors[9-12] in terms of the so-called "hard elasticity."

On stretching the MD specimen, the specimen begins to turn white at *ca.* 10% elongation and this whitening becomes completed at *ca.* 20% elongation. The specimen exhibits no trace of necking with further stretching, but is instead followed by a break at *ca.* 75% elongation that is far less than the breaking elongation at several hundred % elongation in the transverse direction. The specimen shows a marked reduction in apparent density with stretching along the MD. This whitening behavior and apparent density reduction are definitely related to the development of an interlamellar void or a lowered density region, which eventually leads to an appreciable contribution of form birefringence to the dynamic birefringence study of the specimen.[3] This form birefringence was confirmed to be negative in its sign in a previous study on the birefringence of the specimen as a function of % elongation of the specimen in the machine direction and the refractive index of immersion liquid for birefringence measurement.

A more elaborate study on the deformation behavior of the specimen stretched along the MD and TD has been reported elsewhere,[2] and is of crucial importance in accounting for the structural responses of dynamic mechanical dispersions and should be described again for clarity. Figure 1 illustrates the variation in second-order orientation factors of the three principal crystallographic axes of polyethylene crystal with respect to % elongation of the specimen along the MD at room temperature. The orientation factor of the k-th crystal axis is defined as $F_k^0=(3\langle\cos^2\theta_k\rangle-1)/2$ with θ_k being the angle between the k-th crystal axis and the stretching direction. In the unstretched state, the orientation factor of the crystal b-axis, F_b^0, is observed to be approximately -0.5, suggesting that the crystal b-

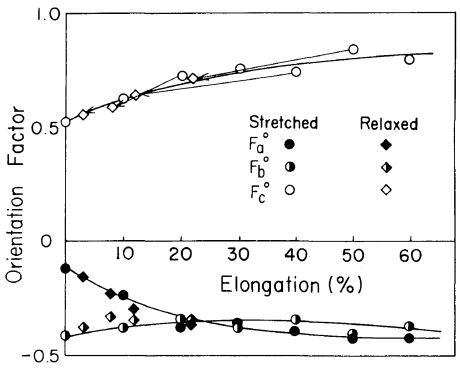

Figure 1. The changes in second-order uniaxial orientation factors of the principal crystallographic axes, F_a^0, F_b^0, and F_c^0, with elongation (%) of the film specimen along the MD.

axis which coincides with the growth direction of the lamellae (lamellar axis) orients perpendicular to the MD. This is in good agreement with the evidence obtained in previous electron microscopic and SAXS studies.[1] As a result of the preferential *c*-axis orientation toward the MD, the orientations of the crystal *a*- and *c*-axis are not random around the lamellar axis; *i.e.* $F_a^0 \neq F_c^0$, as seen in Figure 1. On stretching, the orientation factor F_c^0 increases while F_a^0 decreases, indicating that the crystal *c*- and *a*-axis orient toward and away from the stretching direction, respectively. F_b^0, however, changes slightly in comparison with F_a^0 and F_c^0. These changes in the orientation factors come about primarily from the lamellar untwisting process involving the rotation of localized fragmental lamellar segments instead of a whole unit or crystal grains within the lamella

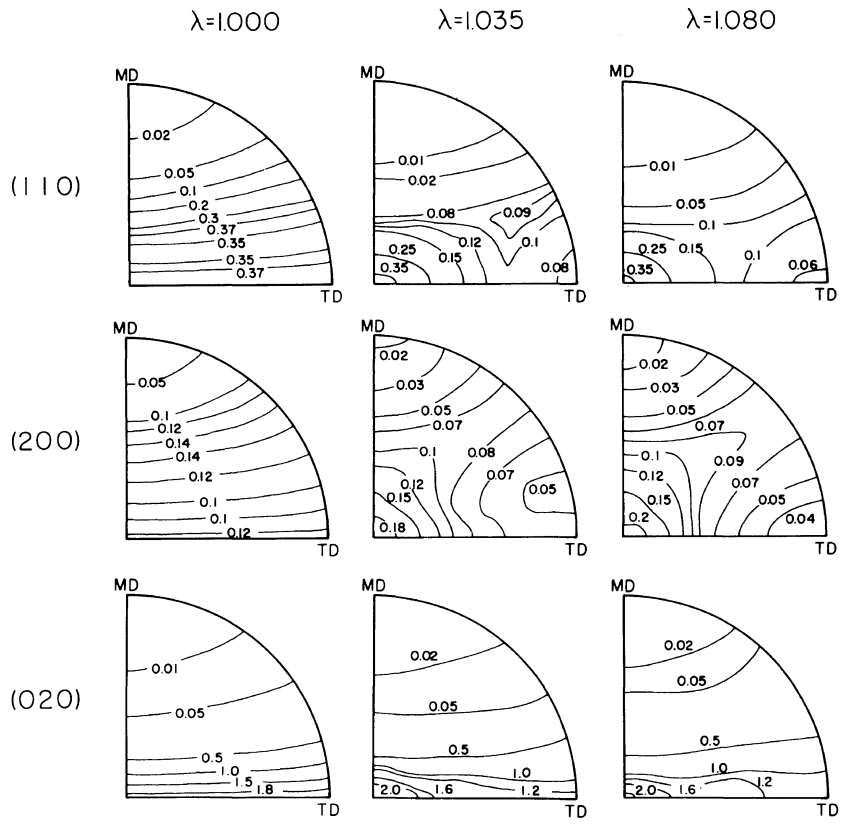

Figure 2. Variations in orientation distributions of the reciprocal lattice vectors of the (110), (200), and (020) crystal planes of the specimen, in terms of the pole figures, with 0, 3.5, and 8.0% elongations along the TD.

around the lamellar axis or the crystal *b*-axis resulting from strain on the part of interlamellar non-crystalline materials, such as tie-chain molecules between the lamellae. The minor change in F_b^0 which increases with increasing % elongation may be attributed to the process of lamellar bending between tie-links in a manner similar to a leaf-spring.[12] Hence, the entire change in these orientation factors can be interpreted in terms of two fundamental processes; *i.e.*, the lamellar untwisting (untwisting of twisted lamellae) and lamellar bending (bending of plate-like lamellae). The former process of lamellar untwisting is believed to be much more important to crystal orientation whereas the latter process of lamellar bending must be more significant to high recoverability from large extension, *i.e.*, this is the property of hard elsticity in the specimen.

Figure 2 shows the variation in the orientation distribution of reciprocal lattice vectors of the *k*-th crystal plane on stretching the specimen along the TD; *i.e.*, the changes in the pole fugure's contour lines of normalized intensity distribution determined by X-ray diffraction, using the (110), (200), and (020) crystal planes. As can be seen in the figure, the orientation distribution of the *k*-th crystal plane in the unstretched state is that of cylindrical symmetry with respect to the MD, as expected from its row-nucleated crystalline texture, but not with respect to the TD. This invalidates the representation of the orientation behavior with stretching along the TD simply in terms of the second-order orientation factor F_k^0 with respect to the TD alone. On stretching along the TD, the orientation distributions of the reciprocal lattice vectors of these crystal planes change in ways such that the distribution maxima accentuate in the thickness direction of the film specimen. Although the contour line for the (020) crystal plane does not appreciably change near the polar region (the region near the MD in the figure), it changes drastically near the equatorial region (the region near the TD in the figure) to align crystal *b*-axis parallel to the thickness direction. On the other hand, variation in the orientation distribution for the (200) crystal plane is comparatively gradual with the elongation ratio. Though a possible deformation mechanism may include a slight orientation of the crystal *a*-axis, intralamellar shearing involving the rotation of the crystal grains around their crystal *a*-axes, particularly in the lamellae oriented parallel to the TD, may be considered as a major process during the stretching of the specimen in the TD up to a yield point of *ca.* 5% elongation.

Dynamic Mechanical Dispersion

Figures 3 and 4 show the temperature dependence of the storage and loss compliance functions of the MD and TD specimens, respectively, over tempera-

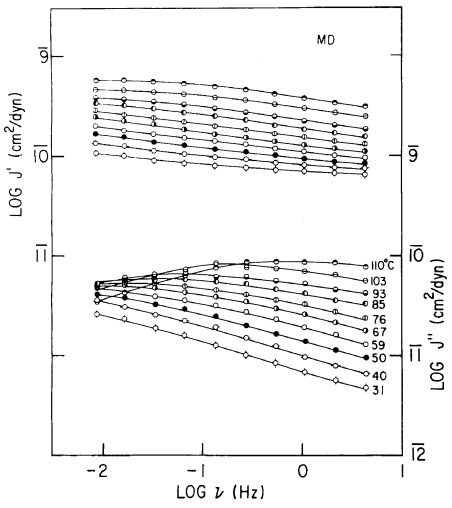

Figure 3. Temperature dependence of the storage and loss compliance functions of the MD specimen.

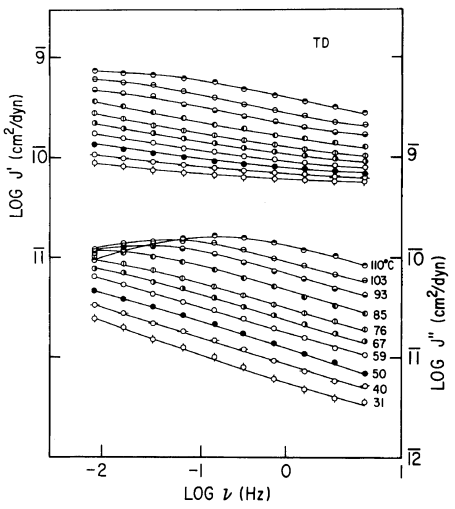

Figure 4. Temperature dependence of the storage and loss compliance functions of the TD specimen.

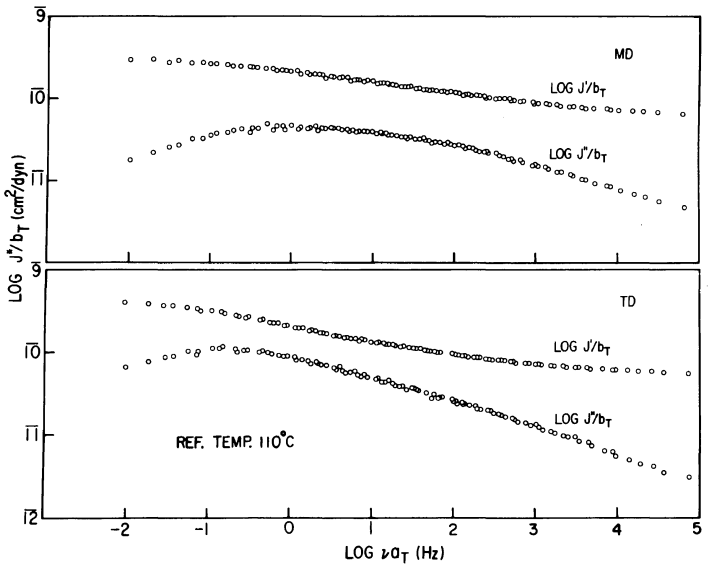

Figure 5. Apparent master curves of the storage and loss compliance functions of the MD and TD specimens reduced to a reference temperature 110°C.

tures ranging from 30 to 110°C. The storage compliance functions for both specimens increase with increasing temperature or decreasing frequency, whereas the loss compliance functions show a somewhat broad dispersion peak at elevated temperatures for both specimens. The rapid increases in the storage compliance as well as in the maximum value of the loss compliance at the dispersion peak with ascending temperature imply that a conventional frequency–temperature superposition simply by a horizontal shift along the logarithmic frequency axis is not likely to be valid, leading to the requirement of a vertical shift in combination with a horizontal shift to obtain a good superposed master curve. Such a superposition is usually arbitrary and thus an attempt has been made to minimize the uncertainty of the procedure by shifting the storage and loss compliance functions simultaneously so that the best fit shift factors can be determined.

Apparent superposed master curves of the storage and loss compliance functions, without taking into account the coexistence of any different retardation mechanisms and being reduced to a common reference temperature of 110°C, are shown in Figure 5 for the MD and TD specimens. As can be seen from this figure, the frequency dispersion, though corresponding to the α mechanical dispersion of polyethylene, is very vast for both specimens in that it is characterized by very broad and asymmetric peak of the loss compliance master curve. Such a broad dispersion may be expected for a system composed of more than a single retardation mechanism. It is worthy to note that the apparent frequency dispersion peak of the loss compliance of the TD specimen appears at somewhat lower frequencies than that of the MD specimen. The activation energies, estimated from the Arrhenius plot of the horizontal shift factor *vs.* reciprocal of the absolute temperature, are found, as shown in Figure 6, to be 24.4 and 36.6 kcal mol^{-1} for the MD specimen and 25.0 and 38.8 kcal mol^{-1} for the TD specimen. These values are in good accord with the reported literature values[13] for the so-called α_1 and α_2 dispersion processes of high-density polyethylene. A further account of these individual processes may no longer be possible unless the consitituent processes are resolved into their separate components. Hence, a breakdown of the vast mechanical dispersion into its individual retardation processes is desirable.

The resolution of the α mechanical dispersion into two components was first introduced by Nakayasu *et al.* on a high-density polyethylene,[14] and later on by Kawai *et al.* on a series of formylated poly(vinyl alcohol)s[5] and on poly(ethylene terephthalate) and

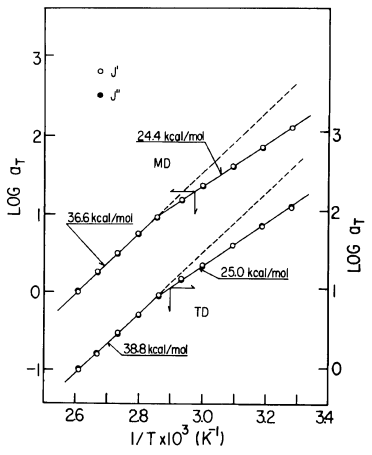

Figure 6. Arrhenius plots of the horizontal shift factors *vs.* the reciprocal absolute temperature for superposing the apparent master curves of storage and loss compliance functions of the MD and TD specimens together with those of the separated master curves.

its related polymers.[6] These procedures are, however, more or less arbitrary, and at present, since there has been no superior procedure, the procedure by Kawai *et al.* has been followed. In this procedure, the following assumptions are adopted; *i.e.*, (i) additivity for assessing the contribution of each retardation (or relaxation) mechanism to the viscoelastic functions, (ii) validity of the time–temperature superposition hypothesis within each retardation (or relaxation) mechanism independent of other mechanisms, and (iii) symmetric loss compliance (or modulus) function of each retardation (or relaxation) mechanism with respect to a logarithmic time scale.

In accordance with the phenomenological theory based on the above three assumptions, the dynamic storage and loss compliance functions may be expressed in terms of the additivity of the j-th retardation mechanisms as follows.

$$J'_T(\omega)=\sum_{j=1}^{m}(\rho/\rho_0)f_j(T,\,T_0)\sum_{i=1}^{n}J_{j,i}(T_0)\times\frac{1}{1+\omega^2\tau_{j,i}{}^2(T_0)a_{T_j}{}^2}=\sum_{j=1}^{m}(\rho/\rho_0)f_j(T,T_0)J'_{j,T_0}(\omega a_{T_j}) \quad (1)$$

$$J''_T(\omega)=\sum_{j=1}^{m}(\rho/\rho_0)f_j(T,\,T_0)\sum_{i=1}^{n}J_{j,i}(T_0)\times\frac{\omega\tau_{j,i}(T_0)a_{T_j}}{1+\omega^2\tau_{j,i}{}^2(T_0)a_{T_j}{}^2}=\sum_{j=1}^{m}(\rho/\rho_0)f_j(T,\,T_0)J''_{j,T_0}(\omega a_{T_j}) \quad (2)$$

where j is the number of retardation mechanisms, and i is the number of retardation elements within the j-th retardation mechanism in which the elements have the identical shift factor a_{T_j} and respective elastic compliance $J_{j,i}$ and retardation time $\tau_{j,i}$. The $f_j(T,\,T_0)$ arises from the identical temperature dependence of the i-th elastic compliance $J_i(T)$ within the j-th mechanism, and $(\rho/\rho_0)f_j(T,\,T_0)$ is a correction factor related to the vertical shift factor b_{T_j} of the time–temperature superposition for the j-th mechanism. The function $f_j(T,\,T_0)$ is expressed in a general form that varies with various j-th mechanisms; for example, if the j-th mechanism has entropic elsticity, the function may be given by (T/T_0).

In addition to the above formulations, a symmetric functional form may be assumed for the frequency dispersion of the loss compliance function of each retardation mechanism, such as a Gaussian-type function with respect to reduced logarithmic frequency, *i.e.*,

$$\log J''_{j,T_0}(\omega a_{T_j})=(A_j-B_j)\times\exp\left[-C_j\{\log(\omega a_{T_j})-\log(\omega a_{T_j})_0\}^2\right]+B_j \quad (3)$$

where $A_j(=\log J''_{j,\max})$ is the maximum loss compliance, $B_j(=\log J''_{j,\min})$ is the asymptotic minimum loss compliance which is negligibly small, $(\omega a_{T_j})_0$ is the reduced frequency at which the maximum loss compliance appears, and C_j is the parameter characterizing the broadness of the j-th mechanical dispersion.

Figure 7 illustrates the superposed master curves of the loss compliance functions for both specimens reduced to a reference temperature of 110°C by shifting the original loss compliance data in Figures 3 and 4 in accordance with the shift factor $a_{T,\alpha_2}(T,\,T_0)$ of the higher temperature α_2 process even for all low temperature data. The Arrhenius plots are, therefore, represented by a single straight line extrapo-

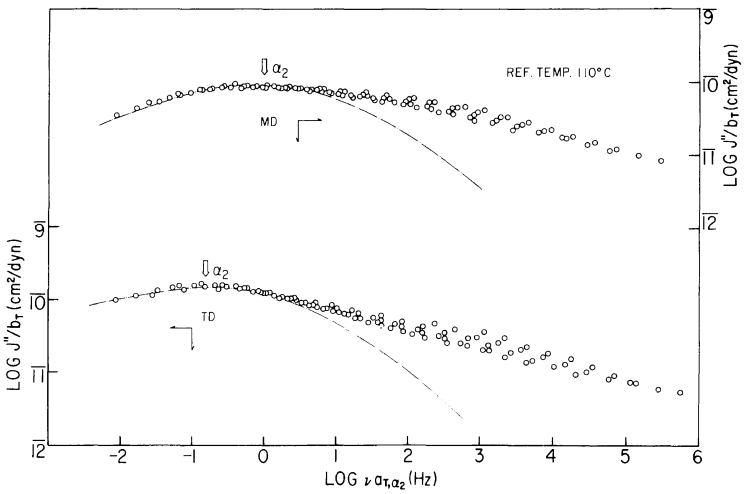

Figure 7. Master curves of the loss compliance functions of the MD and TD specimens superposed in accordance with the horizontal shift factor $a_{T,\alpha_2}(T, T_0)$, of the higher temperature α_2 process reduced to a reference temperature 110°C.

lated at lower temperatures as in Figure 6. Such a superposition may be carried out under the assumption that there exists only one mechanism following the Arrhenius-type retardation process, so that any deviation from the master curve may be responsible for additional retardation mechanisms. It is obvious for both specimens that the lower-frequency portion of the master curve may be superposed very well with a somewhat broad dispersion peak, as indicated by the open arrow, whereas the higher-frequency data are scattered and poorly superposed. This suggests the existence of additional retardation processes at lower temperatures other than the high-temperature α_2 process.

Since the peak position and magnitude of the superposed lower-frequency portion of the master curve is already known, it can be characterized by a Gaussian-type function by adjusting its broadness parameter. The vertical shift has been required for the superposition. Determinations of the broadness parameter and the vertical shift factor of the superposition create arbitrariness. To minimize this, these determinations should be performed by a trial and error method in such a way that the resolved data for the lower-temperature process do not further necessitate any vertical shift in subsequent superpositions. The residual data of the loss compliance functions, after separating the α_2 process, are shown in Figure 8 for both specimens. It is evident that the maximum values of the loss compliance functions maintain almost the same magnitude, implying that no vertical shifts are required in subsequent superpositions for the low-temperature processes, *i.e.*, mostly those of the α_1 process.

Figure 9 shows the superposed master curves of the resolved loss compliance functions for both specimens, obtained by shifting the data in Figure 8

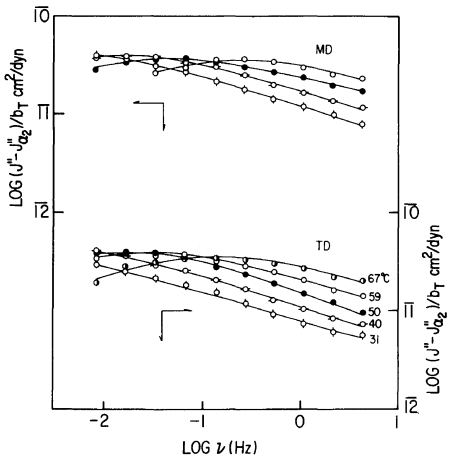

Figure 8. The residual data of loss compliance function after separating the α_2 process of the MD and TD specimens.

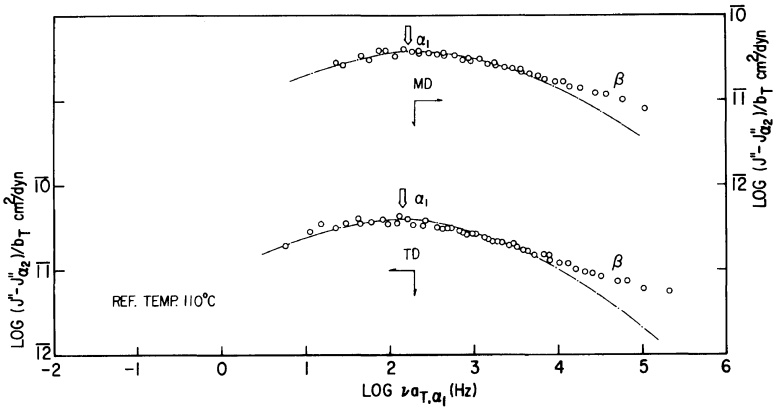

Figure 9. Master curves of the resolved compliance functions of the MD and TD specimens by superposing again with the horizontal shift factors of the lower temperature α_1 process reduced to the same reference temperature 110°C.

horizontally along the logarithmic frequency axis so as to reduce to the same reference temperature of 110°C. The frequency dispersion peaks for both the MD and TD specimens obviously appear nearly within the same frequency region with almost identical peak heights. These resolved loss compliance peaks may also be characterized by Gaussian-type functions for the α_1 process, as indicated by dot-dash lines in the figure, except for further residual portions at the higher-frequency side. These residual portions may arise from the β process. The broadness parameter of the Gaussian-type function for the α_1 process thus evaluated is found to be almost the same for both specimens, suggesting that the α_1 mechanical retardation process contributes to the dynamic mechanical properties of the specimens with an almost equal magnitude. The activation energies estimated on the basis of the Arrhenius plots of the horizontal shift factors *vs.* $1/T$ were found to be 24.4 and 25.0 kcal mol^{-1} for the MD and TD specimens, respectively.

The vertical shift factors required for superposing the apparent and real master curves with and without the resolution, respectively, are plotted against temperatures in Figure 10. Within experimental error, the vertical shift factors for the two cases are in good agreement, and their slopes are a little less steeper than those obtained from the superposition of their dynamic modulus functions but are comparable with those obtained for the low- and medium-density polyethylenes.[15] The arbitrariness

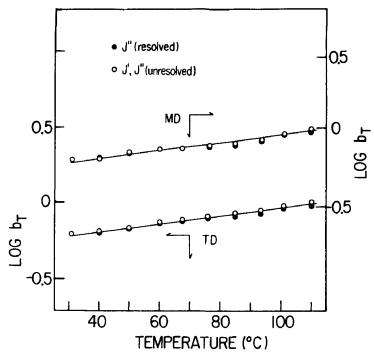

Figure 10. Temperature dependences of the vertical shift factors, $b_T(T, T_0)$, required in the superposition of unresolved and resolved master curves of the storage and loss compliance functions of the MD and TD specimens.

of the procedure is thus not as serious as might be expected.

In order to examine whether or not the resolution procedure is worthwhile, the real and apparent master curves of the loss compliance functions are analyzed in terms of their respective retardation spectra. Figure 11 illustrates the mechanical retardation spectra of the resolved and unresolved dispersions of the α_1 and α_2 processes plotted as functions of retardation time at the reference temperature of 110°C. These mechanical spectra are evaluated in accordance with the deconvolution method reported in a previous paper.[4] Now, one can compare the

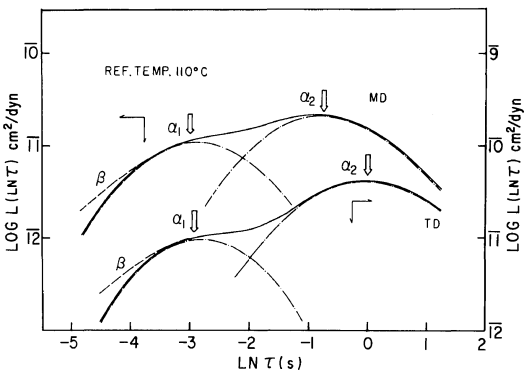

Figure 11. Retardation spectra of unresolved and resolved mechanical dispersions *vs.* logarithmic retardation time for the MD and TD specimens reduced to a reference temperature 110°C.

spectra of the MD and TD specimens so as to see that the spectra of the α_1 process appear within almost the same retardation time range with almost equal retardation intensity for the MD and TD specimens whereas the spectrum of the α_2 process of the TD specimen appears at longer retardation times with greater retardation intensity than that of the MD specimen. Hence, it may be concluded that the α_2 dispersion is more prominent in the TD than in the MD in contrast to the identical α_1 dispersion for both specimens.

Dynamic Optical Dispersion

The dynamic birefringence results obtained simultaneously with the mechanical data are analyzed in terms of real and imaginary components of the complex dynamic stress-optical coefficient function, *i.e.*, M' and M''. Figure 12 shows the temperature dependence M' and M'' for the MD specimen over temperatures ranging from 30 to 110°C. The real component M' at low temperatures remains at negative values, displaying a slight negative maximum with respect to frequency. With ascending temperature, the M' curves turn towards zero and eventually change to positive values. Around 110°C, the M' curve reaches a limiting value of about 1.0×10^{11} cm^2 dyn^{-1} and levels off. The negative M' has been explained as coming from negative form birefringence, whereas the positive M' is attributed to the lamellar unetwisting process involving the rotation of crystal *a*- and *c*-axis around the crystal *b*-axis in such a way that the crystal *c*-axis aligns towards the stretching direction.[2,3]

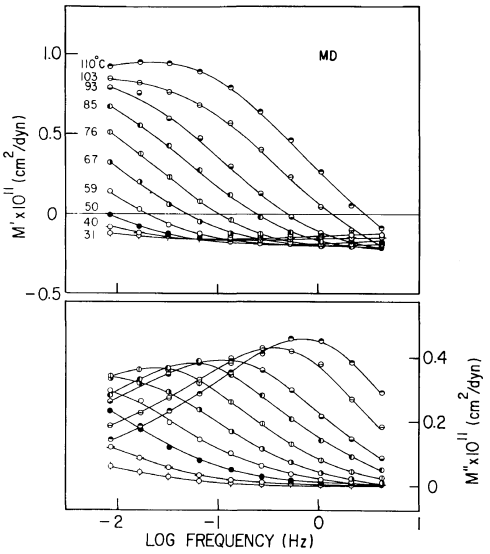

Figure 12. Temperature dependences of real and imaginary components M' and M'' of the complex dynamic stress-optical coefficient function of the MD specimen.

The imaginary component M'' increases with decreasing frequency, but shows frequency dispersion peaks at elevated temperatures. As can be noticed from the figure, the magnitude of the maximum peak increases with ascending temperature, suggesting that a conventional frequency–temperature superposition by simply shifting the data along the logarithmic frequency axis is invalid, leading to the requirement of a vertical shift and also a horizontal shift in the superposition procedure. The same sign of M' and M'' at elevated temperatures implies that the orientational birefringence associated with the lamellar detwisting process lags behind the bulk stress. However, the different sign of M' and M'' at low temperatures or high frequencies should not necessarily mean that this negative form birefringence leads the bulk stress because the birefringence dispersion is not only caused by the lamellar bending on lamellar splaying process but also by a lamellar untwisting process. Unless the contribution of each process to the birefringence dispersion is separated quantitatively, no conventional interpretation of the phase relation is applicable.

The complementary results of the M' and M'' of the TD specimen are illustrated in Figure 13. Contrary to the M' of the MD specimen in Figure 12, the M' has positive values even at low temperatures which increase steadily with decreasing frequency. The increase of M' with decreasing frequency becomes more rapid at elevated temperatures. The M'' also increases with decreasing frequency at low temperatures but shows a dispersion peak at elevated temperatures. The deformation process responsible for the optical dispersion has been explained from a previous dynamic X-ray diffraction study in terms of the intralamellar shearing involving the rotation of crystal grains within the lamellae, *i.e.*, the rotation of crystal *b*- and *c*-axis around the crystal *a*-axis. The same sign of the M' and M'' indicates that the orientational birefringence associated with the intralamellar shearing lags behind the bulk stress. It should be pointed out that the magnitudes of M' as well as of M'' are greater in the TD specimen than in the MD specimen.

A conventional frequency–temperature superposition with a simple horizontal shift along the logarithmic frequency seems no longer valid for the M^* of the TD specimen. Contrary to the storage and loss compliance, the M^* are not sustained either at

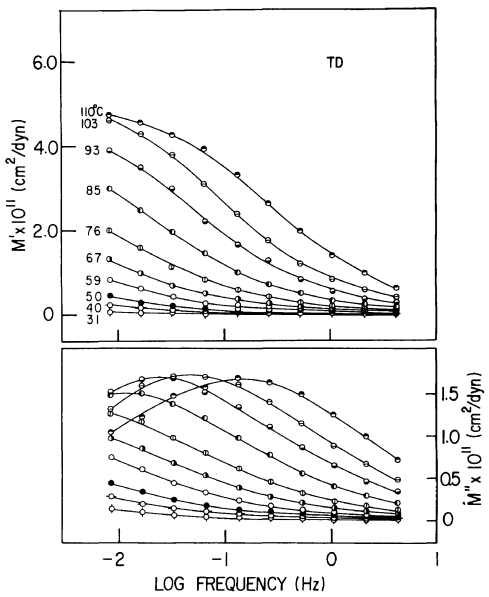

Figure 13. Temperature dependences of real and imaginary components M' and M'' of the complex dynamic stress-optical coefficient function of the TD specimen.

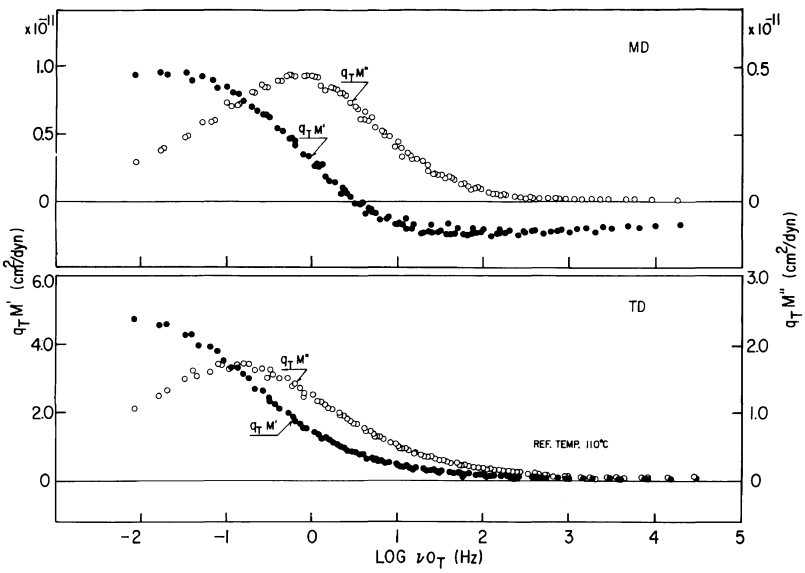

Figure 14. Apparent master curves of the real and imaginary components of the complex dynamic stress-optical coefficient functions of the MD and TD specimens reduced to a reference temperature 110°C.

positive or negative values, changing from positive to negative or *vice versa* depending upon the intrinsic birefringence of the responding constituent units. Thus, the M^* must be ploted in semilogarithmic scale against frequency. The vertical shift in an additive form would lead to resulting vertical shift factors having the same dimension with the M^* which will certainly produce complication and is not desirable as pointed out in a previous paper.[15] Thus, an alternative method for the superposition of such a system is performed by multiplying the M^* with a correction factor q_T in such a way that the corrected stress-optical coefficient $q_T M^*$ may be superposed by a simple horizontal shift along the logarithmic frequency. The physical meaning of the correction factor q_T will resemble the vertical shift factor b_T in mechanical data. The superposed master curves of M^* for both MD and TD specimens reduced to a reference temperature of 110°C, are shown in the upper and lower halves of Figure 14, respectively.

The real component of the superposed master curve $q_T M'$ of the MD specimen is negative at high reduced frequencies. This component gradually changes to become more negative with decreasing frequency at the beginning but takes on positive values at low reduced frequencies. The imaginary component $q_T M''$ exhibits a distinct frequency dispersion peak at a reduced frequency of 1 Hz at which the $q_T M'$ shows an inflection. The dispersion peak of the imaginary component is almost symmetric in shape and is sharper than that of the apparent loss compliance peak in Figure 5. In Figure 15, Arrhenius plots of the horizontal shift factor *vs.* the reciprocal of the absolute temperature can be represented by a straight line whose activation energy is estimated to be 24.4 kcal mol^{-1} which is in good agreement with that of the α_1 mechanical process. This suggests that the lamellar untwisting process dominates in the optical dispersion of the MD specimen.

The $q_T M'$ of the TD specimen was found to be almost zero, in contrast to the negative value of the MD specimen, at high reduced frequencies, but increased greatly with decreasing frequency. The $q_T M''$ also shows a distinct dispersion peak at a reduced frequency of 0.1 Hz which is considerably lower than that of the MD specimen, suggesting that the retardation time of the optical dispersion is longer in the TD than in the MD specimen. The activation energy as estimated on the basis of the Arrhenius theory was, however, found to be 25.0

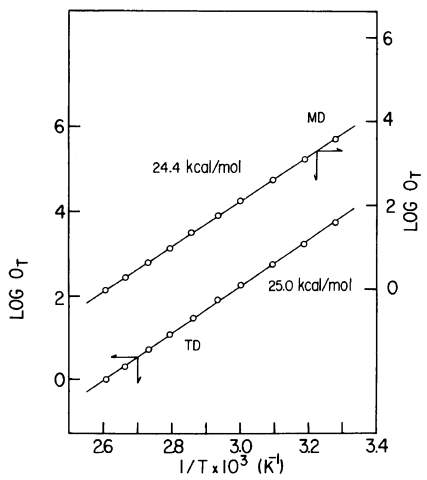

Figure 15. Arrhenius plots of the horizontal shift factors, $o_T(T, T_0)$ *vs.* the reciprocal absolute temperature for superposing the apparent master curves of the real and imaginary components of the dynamic complex stress-optical coefficient functions of the MD and TD specimens, respectively.

kcal mol^{-1} which is comparable with that obtained for the MD specimen as well as with the literature values for the α_1 mechanical dispersion. These facts suggest here again that only one retardation process, *i.e.*, the intralamellar crystal rotation process, is accentuated in the birefringence dispersion. It is worthy to note that the activation energies required to bring about the crystal orientation dispersions of the rotation of the crystal *a*- and *c*-axis around *b*-axis dominating in the MD, and the rotation of the crystal *b*- and *c*-axis around *a*-axis dominating in the TD, are almost the same.

Although the orientational birefringence may not be sensitive to the onset of the rotational vibrations of chain molecules within the crystal lattice, the intrinsic birefringence of the crystal lattice can be influenced by the internal field effect. The reason as to why no prominent birefringence dispersion corresponding to the α_2 process is observed in the Arrhenius plots of the horizontal shift factor *vs.* $1/T$, is that the internal field effect upon the intrinsic birefringence is comparatively smaller than the orientational birefringence at these temperatures or is perhaps diminished in the correction procedure that required a sizable amount of q_T. The q_T required for the superposition is plotted against temperature

in Figure 16 in which q_T changes rather rapidly with temperature. The origin of the temperature dependence of q_T is unclear due to further complication of the combined influences of the temperature dependences of the intrinsic elastic compliance and birefringence of the responding unit. It is felt that the q_T may be related partly to the temperature dependence of the birefringence resulting from the internal field effect and/or crystal disordering effect.

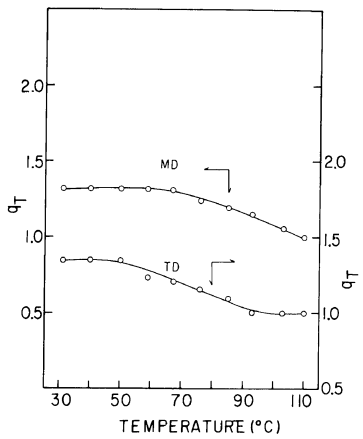

Figure 16. Temperature dependence of the correction factor q_T required for the superposition of the birefringence dispersions of the MD and TD specimens.

To compare the optical dispersion processes of the MD and TD specimens, the optical retardation spectra are computed from the superposed master curves of the imaginary components M'' in accordance with the deconvolution method[4] and are shown in Figure 17. One can envisage that the retardation spectrum for the MD specimen can be characterized by a little sharper distribution with shorter retardation times than that of the TD specimen, resulting in less retardation intensity (the integrated area under the spectral curve) for the MD than for the TD specimen. This suggests that the lamellar untwisting process dominating in the MD specimen is less conspicuous in the optical dispersion than the intralamellar shearing process which dominates in the TD specimen. Judging from the activation energies of the birefringence dispersion for both specimens which are comparable with that of the α_1 mechanical dispersion, it is likely that the orientation-dispersion process may primarily be responsible for the α_1 process rather than the α_2 process. However, the peak positions of these birefringence spectra on the retardation time scale do not correspond to those of the α_1 mechanical dispersion. This implies that the orientation dispersion of the crystals occurs in the vicinities of the α_1 as well as the α_2 mechanical dispersions.

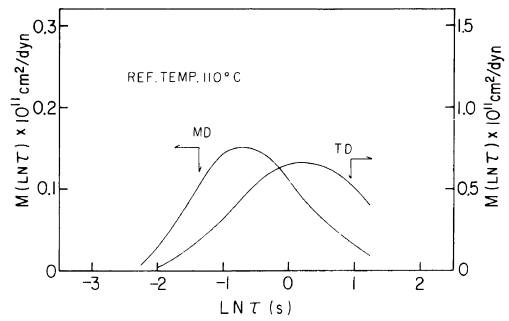

Figure 17. Optical retardation spectra of the birefringence dispersions of the MD and TD specimens reduced to a reference temperature 110°C against logarithmic retardation time.

The real and imaginary components of the stress-optical coefficient functions are recomputed from their respective spectra for the MD and TD specimens and compared with the observed master curves in Figure 18. The calculated curves of $(M' - M'(\infty))$ have greater magnitudes than the observed ones but their shapes, especially for the MD specimen, are similar to the observed master curves $q_T M'$. The residual curve substracting the calculated value from the observed ones for the MD specimen is shown by a dash-dot line in the same figure. The substracted curve has negative value throughout the range of reduced frequency. Instead of being frequency independent, the curve varies slightly with the reduced frequency. This implies that, besides the instantaneous term $M'(\infty)$ of the crystal orientation process,[4] an additional contribution of the lamellar bending or lamellar splaying process which gives rise to the negative form birefringence should be taken into account for the negative value of the substracted curve. The calculated M'' agrees well, within the experimental error, with the observed $q_T M''$, indicating not only the good accuracy of the deconvolution method,[4] but also that the contribution of the lamellar bending or lamellar splaying process is in

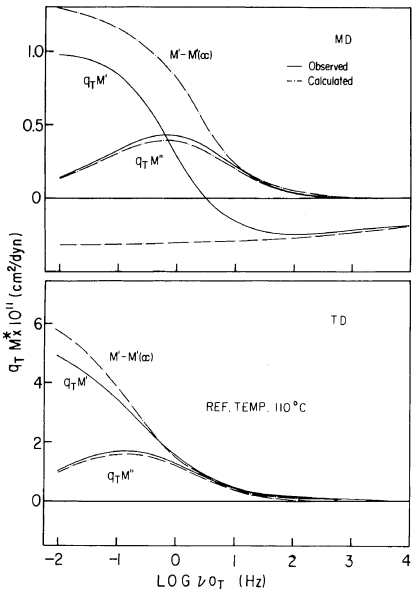

Figure 18. Comparison of the calculated and observed complex stress-optical coefficients of the MD and TD specimens.

phase with the bulk stress. In other words, the contribution of the lamellar bending or lamellar splaying process may not be significant to the α mechanical dispersion, but rather more crucial to the β mechanical dispersion.

For the TD specimen, the calculated and observed M'' are also consistent with each other, but though the calculated $(M'-M'(\infty))$ agrees well with the observed $q_T M'$ at high reduced frequencies, it deviates remarkably from the observed value at lower reduced frequencies corresponding to higher temperature data. The discrepancy at higher temperature data may be due partly to the uncertainty of q_T or to the computational error involving the deconvolution procedure for evaluating the spectrum which usually necessitates that the ends of the imaginary component M'' approach zero for the convergence of integration during the Fourier transformation.

Acknowledgements. This series of rheo-optical studies on the deformation mechanism of semicrystalline polymers has been supported in part by a grant from the U.S.-Japan Cooperative Research Program, of the National Science Foundation and the Japan Society for Promotion of Science. The authors are also indebted to the Nippon Gosei Kagaku Co., Ltd., Osaka, Japan, and the Dai-Cell Co., Ltd., Osaka, Japan, for financial support through a scientific grant.

REFERENCES

1. T. Hashimoto, K. Nagatoshi, A. Todo, and H. Kawai, *Polymer*, **17**, 1063 (1976).
2. S. Suehiro, T. Yamada, T. Kyu, K. Fujita, T. Hashimoto, and H. Kawai, *Polym. Eng. Sci.*, **19**, 929 (1979).
3. T. Kyu, N. Yasuda, S. Suehiro, T. Hashimoto, and H. Kawai, *Polymer*, in press.
4. T. Kyu, S. Suehiro, N. Nomura, and H. Kawai, *J. Polym. Sci., Polym. Phys. Ed.*, in press.
5. M. Nakatani, K. Iijima, A. Suganuma, and H. Kawai, *J. Macromol. Sci.-Phys.*, **B2(1)**, 55 (1968).
6. K. Tajiri, Y. Fujii, M. Aida, and H. Kawai, *J. Macromol. Sci.-Phys.*, **B4(1)**, 1 (1970).
7. T. Kyu, N. Yasuda, M. Tabushi, S. Nomura, and H. Kawai, *Polym. J.*, **7**, 108 (1975).
8. A. Keller and M. J. Machin, *J. Macromol. Sci.-Phys.*, **B1**, 41 (1967).
9. E. S. Clark, "Structure and Properties of Polymer Films," R. W. Lentz and R. S. Stein Ed., Plenum Press, New York, N.Y., 1973, p 267.
10. R. G. Quynn and H. Brody, *J. Macromol. Sci., Phys.*, **B5**, 721 (1971).
11. B. S. Sprague, *J. Macromol. Sci., Phys.*, **B8**, 157 (1973).
12. S. L. Cannon, G. B. McKenna, and W. O. Statton, *J. Polym. Sci., Macromol. Rev.*, **11**, 209 (1976).
13. J. D. Hoffman, G. Williams, and E. Passaglia, *J. Polym. Sci., C*, **14**, 173 (1966).
14. H. Nakayasu, H. Markovitz, and D. J. Plazek, *Trans. Soc. Rheol.*, **5**, 261 (1961).
15. T. Kyu, N. Yasuda, S. Suehiro, S. Nomura, and H. Kawai, *Polym. J.*, **8**, 565 (1976).